REPORT DOCUMENTATION PAGE

Form Approved
OMB No. 0704-0188

1. REPORT DATE *(DD-MM-YYYY)*	**2. REPORT TYPE**	**3. DATES COVERED** *(From - To)*
22-09-2006	Conference Paper PREPRINT	2006

Data-Based Control of a Free-Free Beam in the Presence of Uncertainty (PREPRINT)

5a. CONTRACT NUMBER

5b. GRANT NUMBER

5c. PROGRAM ELEMENT NUMBER

Tannen S. VanZwieten, Gregory M. Bower,* Seth L. Lacy**

5d. PROJECT NUMBER

5e. TASK NUMBER

5f. WORK UNIT NUMBER

7. PERFORMING ORGANIZATION NAME(S) AND ADDRESS(ES)

University of Wyoming
College of Engineering
1000 E. University Ave
Laramie, WY 82071

Pennsylvania State University*
College of Engineering

8. PERFORMING ORGANIZATION REPORT NUMBER

9. SPONSORING / MONITORING AGENCY NAME(S) AND ADDRESS(ES)

Air Force Research Laboratory**
Space Vehicles
3550 Aberdeen Ave SE
Kirtland AFB, NM 87117

10. SPONSOR/MONITOR'S ACRONYM(S)
AFRL/VSSV

11. SPONSOR/MONITOR'S REPORT NUMBER(S)
AFRL-VS-PS-TP-2007-1003

12. DISTRIBUTION / AVAILABILITY STATEMENT
Approved for public release; distribution is unlimited. (Clearance #VS06-0630)

13. SUPPLEMENTARY NOTES
Accepted for publication in the Proceedings of the American Control Conference; 11-13 Jul 07, NY, NY

Government Purpose Rights

14. ABSTRACT

Linear control development is typically based on deterministic models that approximate the system under consideration. This approach neglects uncertainty in the system response. System uncertainty can arise from a number of sources including disturbances, noise, un-modeled dynamics, and nonlinearity. This may result in a reduction in performance or even instability in the closed loop system. The goal of this research is to account for measured uncertainty in control design. Our approach is to tune a baseline controller using a cost function that balances performance and robustness given measured system uncertainty. The approach is demonstrated on a free-free beam, with the goal of mitigating the flexural vibration. A lumped mass model is tuned to match the experimentally measured Frequency Response Function (FRF) of an experimental beam. This evaluation model and a reduced order model are used to approximate the beam dynamics. The baseline (LQG) controller is designed around the reduced order model of the beam. This controller is tuned according to the proposed cost function using the FRF and postulated variance. The cost function includes closed loop performance and stability robustness metrics. The resulting baseline and tuned controllers are evaluated on lumped mass models consistent with the measured data and uncertainty.

15. SUBJECT TERMS
Linear, Deterministic Models, Disturbances, Noise, Nonlinearity, Baseline Controller, Robustness, Flexural Vibration, FRF, LQG, System Uncertainty, Measured Uncertainty

16. SECURITY CLASSIFICATION OF:			**17. LIMITATION OF ABSTRACT**	**18. NUMBER OF PAGES**	**19a. NAME OF RESPONSIBLE PERSON**
a. REPORT	**b. ABSTRACT**	**c. THIS PAGE**			Seth L. Lacy
Unclassified	Unclassified	Unclassified	Unlimited	9	**19b. TELEPHONE NUMBER** *(include area code)* 505-853-3176

Data-Based Control of a Free-Free Beam in the Presence of Uncertainty

Tannen S. VanZwieten, Gregory M. Bower and Seth L. Lacy

Abstract— **Linear control development is typically based on deterministic models that approximate the system under consideration. This approach neglects uncertainty in the system response. System uncertainty can arise from a number of sources including disturbances, noise, unmodeled dynamics, and nonlinearity. This may result in a reduction in performance or even instability in the closed loop system. The goal of this research is to account for measured uncertainty in control design. Our approach is to tune a baseline controller using a cost function that balances performance and robustness given measured system uncertainty. The approach is demonstrated on a free-free beam, with the goal of mitigating the flexural vibration. A lumped mass model is tuned to match the experimentally measured Frequency Response Function (FRF) of an experimental beam. This evaluation model and a reduced order model are used to approximate the beam dynamics. The baseline (LQG) controller is designed around the reduced order model of the beam. This controller is tuned according to the proposed cost function using the FRF and postulated variance. The cost function includes closed loop performance and stability robustness metrics. The resulting baseline and tuned controllers are evaluated on lumped mass models consistent with the measured data and uncertainty.**

I. INTRODUCTION

Deterministic models are routinely developed as the basis for linear control development by approximating the system under consideration. However, no model is perfect. Uncertainty is introduced to the system via disturbances, noise, unmodeled dynamics, and nonlinearity. This can result in a reduction in performance or even instability in the closed loop system.

System uncertainty can be particularly significant with flexible structures. Since flexible structures are infinite dimensional, implementable control designs must be reduced order.

One example of a large flexible structure is the Deployable Optical Telescope (DOT) at the Air Force Research Laboratory on Kirtland Air Force Base (shown in Figure 1). Data based models were created for this lightly damped, modally dense structure [1]. Variance information was captured to quantify the uncertainty. DOT's optical requirements necessitate the use of a very precise controller, but this cannot be at the expense of stability.

This work was supported by the Air Force Research Laboratory, Space Vehicles Directorate, Kirtland Air Force Base, NM

Tannen S. VanZwieten is a PhD Candidate in Electrical Engineering at the University of Wyoming tvanzwie@uwyo.edu

Gregory M. Bower is a PhD Candidate in Electrical Engineering at Pennsylvania State University Fox-13@psu.edu

Seth L. Lacy is with the Air Force Research Laboratory, Space Vehicles Directorate, Kirtland Air Force Base, NM seth.lacy@kirtland.af.mil

Fig. 1. AFRL's Deployable Optical Telescope

This paper develops the idea of using measured FRF and variance information to tune a baseline controller. The goal of the tuning algorithm is to find a controller that can account for measured system uncertainty.

Our approach is to tune a baseline controller using a cost function that attempts to balance closed loop performance and robustness given measured system uncertainty. In the absence of uncertainty, the H_2 cost function gives optimal performance. However, there are no guaranteed stability margins for a H_2 (or LQG) controller [2], [3], and in the presence of uncertainty the standard H_2 optimal controller has been found not to be sufficiently robust for practical applications [4]. Therefore, a Nyquist-criteria based cost function will be included with the H_2 cost to form the total cost. A similar technique was developed in [5]. The controller will be optimized based on the FRF and postulated variance information. The inclusion of FRF variance allows the stability and performance of the closed loop system to be evaluated in terms of the probability of meeting a performance goal and the probability of being stable.

Our analysis is demonstrated on a free-free beam, with the goal of mitigating the flexural vibration. Similar to DOT, the free-free beam contains an infinite number of states, forcing the controller design to be based on a ROM. The controller development will be shown here for the SISO case, but the Generalized Nyquist Stability Criterion [6] would allow it to be extended for MIMO systems.

This paper begins in Section II with a description of the experimental setup, including the spatial model, data collection and validation. The Frequency Response Function

collected from the experiment is used to tune a lumped mass model that is developed in Section III. A ROM of the lumped mass model is also presented in Section III. This is used to approximate the beam dynamics and serves as the basis for the development of the baseline (LQG) controller in Section IV. Section V introduces postulated uncertainty that is consistent with the unperturbed and perturbed beam models. In Section VI the controller design is presented in terms of cost functions and their corresponding sensitivities. Finally, numerical simulations are presented in Section VII, followed by conclusions and future work in Section VIII.

II. EXPERIMENT

A. Spatial Model

A spatial model describes the physical characteristics of a structure, and serves as the basis for the theoretical model development [7]. Here, a free-free beam is chosen for analysis, with a control input applied at $x = a$, as shown in Figure 3. The physical characteristics of this structure are

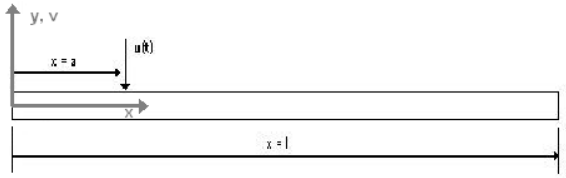

Fig. 2. Free-Free Beam with Force Applied at $x = a$

given below.

Dimensions

length: $l = 1.27$ [m]
width: $w = 0.0508$ [m]
thickness: $t = 0.0127$ [m]

Material properties (aluminum)

Young's Modulus: $E = 6.7569e10$ [Pa]
density: $\rho = 2767.99$ [kg/m^3]

B. Setup

The beam was suspended from the ceiling like a pendulum to simulate free-free boundary conditions, as shown in Figure 3. Control input was applied via a 5 lbf electrodynamic shaker and a load cell was used to measure this input force.

The output measurement point was collocated with the driving point. The velocity/force response was measured with a laser vibrometer.

C. Driving and Measuring Point Location

The location of the driving/measuring point was strategically chosen based on the first four mode shapes. These shapes, calculated from Euler-Bernoulli free vibration solution [8], are shown in Figure 4 and Figure 5. The small green circle denotes the chosen I/O location, $a = 21.27$ cm. This point was chosen near the peak of third and fourth modes so that the magnitude of vibration for these modes was comparable to that of the first and second modes (which is inherently larger). This choice facilitates the excitation of

Fig. 3. Experimental Setup

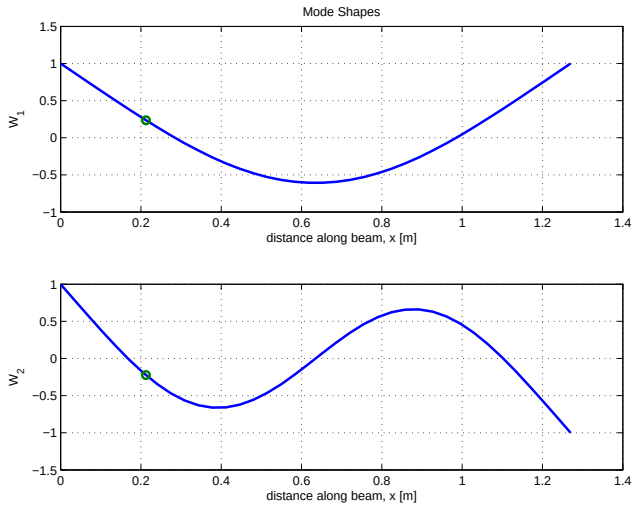

Fig. 4. Mode Shapes: First and Second Modes

the smaller modes in such a way that the output response will not be dominated by larger amplitude modes.

D. Frequency Response Function

Three sets of frequency response functions were collected with the following frequency intervals and bandwidths,

$$\begin{aligned} \triangle f_1 &= 0.25 \text{ Hz} \qquad \text{BW}_1 : 0 - 800 \text{ Hz}, \\ \triangle f_2 &= 0.125 \text{ Hz} \qquad \text{BW}_2 : 0 - 400 \text{ Hz}, \\ \triangle f_3 &= 0.0625 \text{ Hz} \qquad \text{BW}_3 : 0 - 200 \text{ Hz}. \end{aligned}$$

The mobility (velocity/force FRF) collected experimentally was averaged over all three data sets, as shown in Figure 6. This was integrated to give the compliance (displacement/force). All future calculations are based on the average FRF values for compliance.

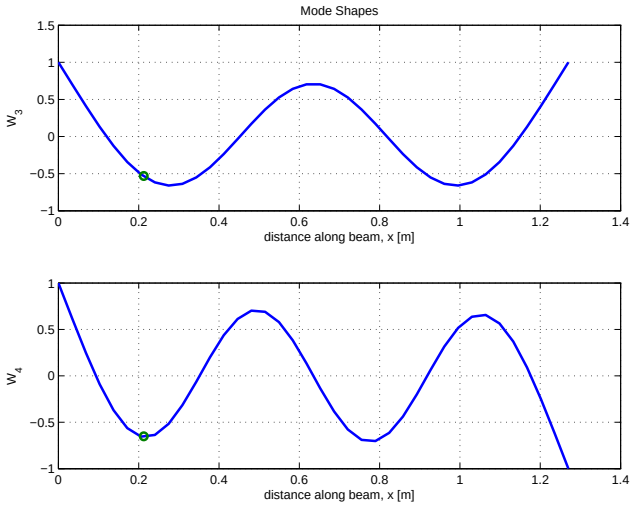

Fig. 5. Mode Shapes: Third and Fourth Modes

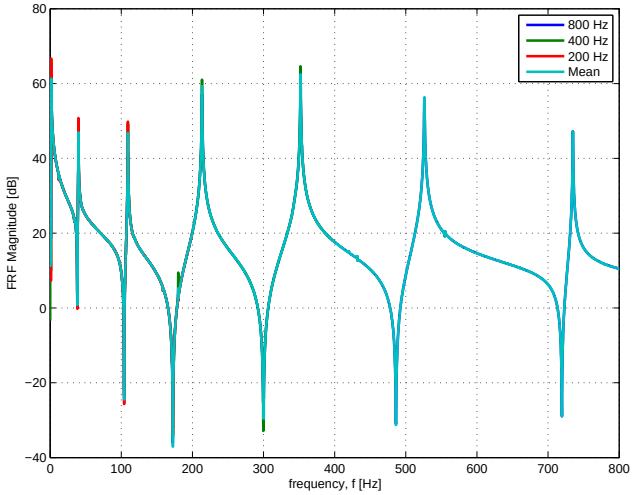

Fig. 6. FRF for Free-Free Beam

E. Validation

For any beam there will be an infinite number of normal modes, where each mode is associated with a natural frequency. The mode of lowest frequency is found from the experimental compliance to occur at 1.5 Hz and is a rigid body mode rather than a flexural mode. This mode is associated with the support conditions, and in this case corresponds to a pendulum-like motion of the beam. For our analysis, the first four dominant *flexural* modes are selected from the FRF,

$$\begin{aligned} f_1 &= 39.75 \text{ Hz}, \\ f_2 &= 109.39 \text{ Hz}, \\ f_3 &= 213.5 \text{ Hz}, \\ f_4 &= 352.0 \text{ Hz}. \end{aligned} \tag{1}$$

These frequencies correspond to points of maximimum response of the average FRF. The sharp peaks at these frequencies indicate that the beam is very lightly damped. Theoretical natural frequencies [8] matched experiment values for the first four modes with less than one percent error.

III. LUMPED MASS MODEL

The lumped mass model development relies on the spatial model of the beam given in Section II-A. This model gives transient response characteristics of the beam in addition to the modal model (steady state).

For a lumped mass model, the beam is split into n_e elements with $n_n = n_e + 1$ nodes, as shown in Figure 7. Each node is defined by one translational and one rotational

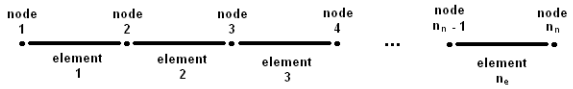

Fig. 7. Elements and Nodes for a Lumped Mass Model

degree of freedom, giving the entire beam $2n_n$ degrees of freedom and $4n_n$ states. Each element is defined to have a length $l_e = \frac{l}{n_e}$.

A. Mass Matrix

A simple lumped mass matrix is chosen, where the mass of each element is chosen in proportion to the number of elements in the model. This is known as an inconsistent-mass matrix, since it is not fashioned from a set of shaping and displacement functions such that it is consistent with the stiffness matrix [9]. The mass applied to the node on the end is given by

$$m_e^{\text{end}} = \frac{\rho A l_e}{2}, \tag{2}$$

corresponding to half the mass of the adjoining element. For all other elements the mass is given by

$$m_e = \rho A l_e, \tag{3}$$

since there are two adjoining elements. The mass moment of inertia for each element about the node is found by taking the inertia of half of the adjoining element(s) about the node. In the case of the end nodes, where the node connects to only one element, we find

$$I_e^{\text{end}} = \frac{\rho A l_e^3}{24}. \tag{4}$$

For all other nodes, the inertia corresponds to that of *two* half elements taken about the node of interest, and hence the above quantity is doubled,

$$I_e = \frac{\rho A l_e^3}{12}. \tag{5}$$

The mass/inertia matrix for the entire beam is given by

$$M = \text{diag}\left[\, m_e^{\text{end}} \;\; I_e^{\text{end}} \;\; m_e \;\; I_e \;\; \ldots \;\; m_e \;\; I_e \;\; m_e^{\text{end}} \;\; I_e^{\text{end}} \,\right], \tag{6}$$

where $M \in \mathbb{R}^{2n_e \times 2n_e}$.

B. Stiffness Matrix

The stiffness assigned to each nodal DOF corresponds to the stiffness of the element(s) neighboring the node of interest. Therefore the stiffness of each element must be characterized and then related to the nodal linear and angular displacement.

The forces and moments are applied at the nodes on either end of the element, $x_e = 0$ and $x_e = l_e$, as shown in Figure 8. The forces and moments at nodes 1 and 2 are related to

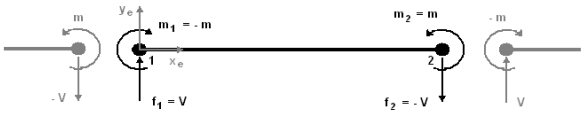

Fig. 8. Forces and Moments on a Beam Element

the stiffness of the element by

$$\begin{bmatrix} f_1 \\ m_1 \\ f_2 \\ m_2 \end{bmatrix} = \frac{EI}{l_e^3} \begin{bmatrix} 12 & 6l_e & -12 & 6l_e \\ 6l_e & 4l_e^2 & -6l_e & 2l_e^2 \\ -12 & -6l_e & 12 & -6l_e \\ 6l_e & 2l_e^2 & -6l_e & 4l_e^2 \end{bmatrix} \begin{bmatrix} d_1 \\ \phi_1 \\ d_2 \\ \phi_2 \end{bmatrix}. \quad (7)$$

The shape functions corresponding to (7) illustrate the effect of nodal displacements and rotations on the transverse displacement of a given element along its length [10]. The plot of the shape functions along the length of the beam is shown in Figure 9.

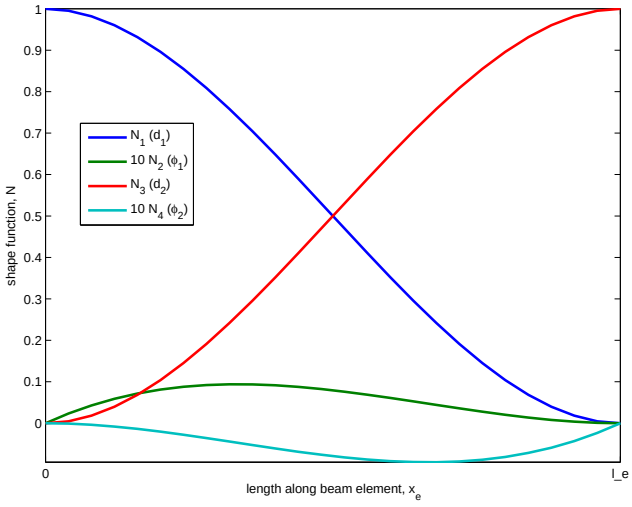

Fig. 9. Shape Functions for a Beam Element

By definition, the stiffness is the force divided by the displacement, so from (7) we see that the element stiffness is simply

$$K_e = \frac{EI}{l_e^3} \begin{bmatrix} 12 & 6l_e & -12 & 6l_e \\ 6l_e & 4l_e^2 & -6l_e & 2l_e^2 \\ -12 & -6l_e & 12 & -6l_e \\ 6l_e & 2l_e^2 & -6l_e & 4l_e^2 \end{bmatrix}, \quad (8)$$

as shown in [11].

For a beam that contains multiple elements, the stiffnesses for each element given by (8) must be assembled such that the nodes of the entire beam are represented in a single matrix. Note that the first two rows/columns of K_e correspond to the linear and angular stiffness of node 1, while the last two rows/columns correspond to node 2. Also note that node 2 of an element represents the same node as node 1 of the adjoining element, provided that there is an element attached to either end (i.e., the node considered does not represent a boundary condition).

The block diagonal matrices of the stiffness for each node with zeros at all other nodes are summed over all nodes to give the stiffness matrix for the entire beam.

C. Equation of Motion

The equation of motion for the lumped-mass beam is

$$M\ddot{\hat{d}}(t) + C\dot{\hat{d}}(t) + K\hat{d}(t) = F(t), \quad (9)$$

where $\hat{d} = [\ d_1 \quad \phi_1 \quad d_2 \quad \phi_2 \quad \ldots \quad d_{n_m} \quad \phi_{n_m}\ ] \in \mathbb{R}^{2n_m}$ is the linear and angular displacement at each node and $F \in \mathbb{R}^{2n_m}$ is the vector of forces and moments applied at each node. Defining $x_1 \triangleq \hat{d}$, $x_2 \triangleq \dot{\hat{d}}$, and $x \triangleq [x_1\ x_2]^{\mathrm{T}}$, this may be re-written in state space form as

$$\dot{x}(t) = Ax(t) + Bu(t), \quad (10)$$

where

$$\begin{aligned} A &= \begin{bmatrix} 0_{2n_m \times 2n_m} & I_{2n_m \times 2n_m} \\ -M^{-1}K & -M^{-1}C \end{bmatrix}, \\ B &= \begin{bmatrix} 0_{2n_m \times 2n_m} & 0_{2n_m \times 2n_m} \\ 0_{2n_m \times 2n_m} & M^{-1} \end{bmatrix}, \\ u(t) &= \begin{bmatrix} 0_{2n_m} \\ F(t) \end{bmatrix}. \end{aligned} \quad (11)$$

D. Tuning

The lumped mass FRF converges to the experimental FRF as the number of nodes is increased. The model was tuned by adjusting the damping coefficients along the modes. The addition of damping results in a stable open loop system, which is important for the existence of the H_2 norm that will be used as the performance metric in the controller cost function. This stable open loop assumption is also an important consideration for the Nyquist-based stability metric.

The FRF for the lumped mass model with 55 elements and linear and angular damping coefficients of $c = 0.1808$ and $c = 1.33e-6$, resp. is shown in Figure 11.

Since the focus for the model development and control in this paper is on the flexural modes of vibration, the rigid body mode was eliminated via a high pass Butterworth filter. This is shown in Figure 10 for the lumped mass model. The same filter was applied to the experimental data.

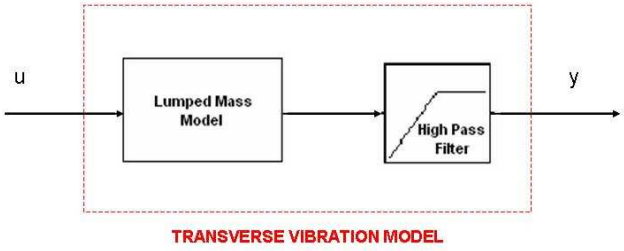

Fig. 10. Eliminate Rigid Body Mode With a High Pass Filter

E. Reduced Order Model

A ROM is developed to approximate the dynamics given by the lumped mass model in (10). The purpose is to reduce the model's computational complexity as much as possible while retaining the major system characteristics. The baseline and robust controllers will be developed around the ROM.

The lumped mass model was transformed into modal form. The states with a small contribution to the input-output response were identified, isolated, and eliminated. The FRF for a ROM of order $n_r = 12$ and a lumped mass model with 55 elements (220 states) is plotted alongside the beam's experimental FRF in Figure 11. The SISO ROM is represented by (A_r, B_r, C_r, D_r) with $A_r \in \mathbb{R}^{n_r \times n_r}$, $B_r \in \mathbb{R}^{n_r}$, $C_r \in \mathbb{R}^{n_r}$, and $D_r \in \mathbb{R}$.

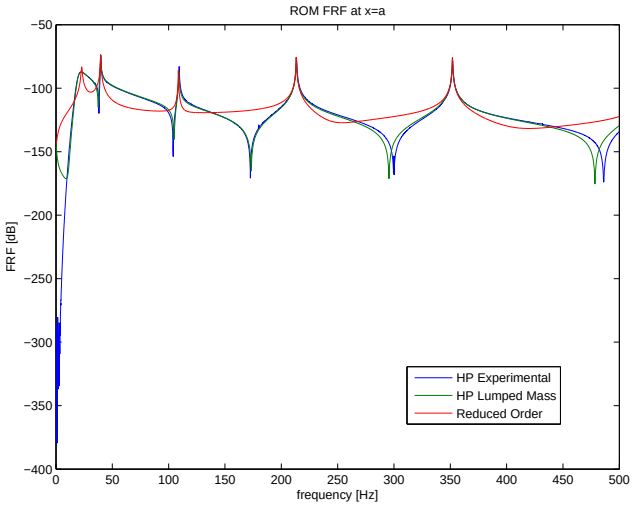

Fig. 11. Lumped Mass Model, Reduced Order Model and Experimental Compliances

IV. BASELINE CONTROLLER

A. Linear Quadratic Gaussian

An LQG controller may be written in state space form as

$$\dot{x}_c(t) = A_c x_c(t) + B_c u_c(t) \quad (12)$$
$$u = C_c x_c(t) \quad (13)$$

where $A_c \in \mathbb{R}^{n_r x n_r}$, $B_c \in \mathbb{R}^{n_r x 1}$, $C_c \in \mathbb{R}^{1 x n_r}$, $D_c \in \mathbb{R}$, and

$$A_c = A_r - B_r K - L C_r \quad (14)$$
$$B_c = L \quad (15)$$
$$C_c = -K. \quad (16)$$

where L is the Kalman filter gain and K is the LQR static state feedback gain.

B. Parameterization

The baseline controller is developed using the SISO ROM that contains n_r states. Hence, the standard LQG form results in $n_r^2 + n_r$ parameters that will need to be tuned using the algorithm in the following section. Conversely, for the same controller in modal form, there exist $3n_r$ parameters to estimate. Therefore by transforming the baseline controller into modal form there is a reduction of $n_r^2 - 2n_r$ parameters. For a ROM with $n_r = 12$ states, the LQG controller in standard form results in 156 parameters, but once transformed into modal form there are only 36 parameters – a reduction of 120 parameters.

V. UNCERTAINTY

Uncertainty in systems is caused by a number of different sources, including disturbances, noise, unmodeled dynamics and nonlinearities. The effect of this uncertainty may be a reduction in performance or even instability of the closed loop system.

We introduce uncertainty in the form of postulated variance information. The variance is the square of this standard deviation, σ^2. This standard deviation may be used to define confidence intervals around the experimental FRF. For example, a 95% confidence interval is given by 1.96σ and a 99% confidence interval is given by 2.58σ.

For our purposes, the postulated variance is simply calculated from the compliances of unperturbed and perturbed lumped mass models that will be used to test the controller robustness in Section VII. In particular, 1.96σ was defined such that it smoothly encompasses the deviation of the perturbed system, as shown in Figure 12. This corresponds to a 95% confidence interval around the displacement of the unperturbed system, shown in Figure 13.

VI. ROBUST CONTROLLER DESIGN

The robust controller design considered here augments an H_2 performance cost with a Nyquist-based stability cost. Both cost functions are data-based, hence the tuning relies completely on the FRF. Note that for the remainder of the paper the specific dependence on $j\omega$ or t, where obvious, may be omitted for simplicity of exposition.

A. Closed Loop System

Let the state space representation of the ROM be represented by,

$$\dot{x}_r = A x_r + B_u u,$$
$$z = C_z x_r + D_{zu} u, \quad (17)$$
$$y = C_y x_r + D_{yu} u,$$

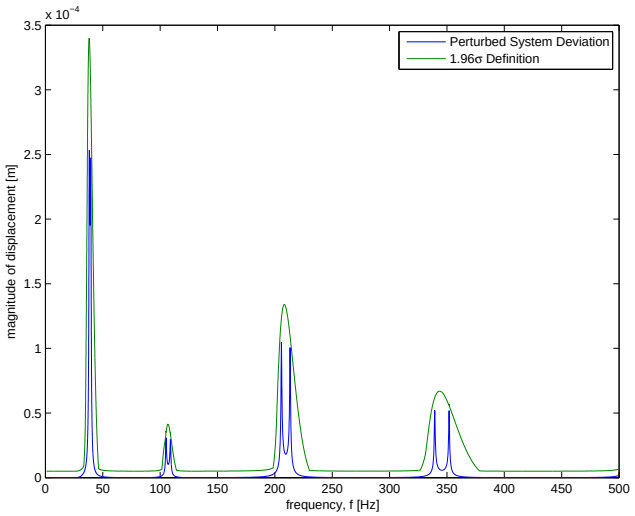

Fig. 12. Postulated Standard Deviation

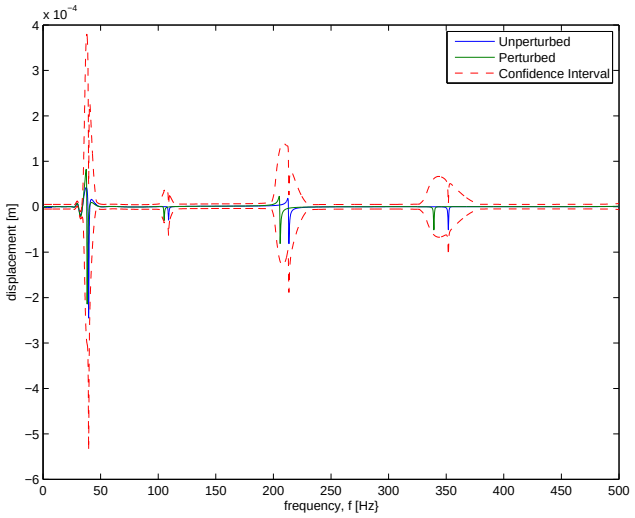

Fig. 13. Perturbed and Unperturbed Systems with 95% Confidence Interval

where x_r denotes the state of the ROM and z is a performance measure. The corresponding transfer functions are given by

$$G_{yu}(s) = C_y\left(sI - A\right)^{-1}B_u + D_{yu}, \quad (18)$$
$$G_{zu}(s) = C_z\left(sI - A\right)^{-1}B_u + D_{zu}. \quad (19)$$

Combing the above ROM plant equations from (17) with the controller given by (12) and (13), the closed loop state equation becomes

$$\begin{bmatrix}\dot{x}\\ \dot{x}_c\end{bmatrix} = \begin{bmatrix}A & B_uC_c\\ B_cC_y & (A_c + B_cD_{yu}C_c)\end{bmatrix}\begin{bmatrix}x\\ x_c\end{bmatrix} \quad (20)$$

and the closed loop performance and output equations are

$$z = \begin{bmatrix} C_z & D_{zu}C_c \end{bmatrix}\begin{bmatrix} x\\ x_c\end{bmatrix}, \quad (21)$$
$$y = \begin{bmatrix} C_y & D_{yu}C_c \end{bmatrix}\begin{bmatrix} x\\ x_c\end{bmatrix}, \quad (22)$$

respectively. The above closed loop matrices are denoted by $A^{(cl)}$, $C_z^{(cl)}$, and $C_y^{(cl)}$.

B. Cost Functions

The data-based performance cost is taken as the weighted sum of the H_2 for the output and performance variables,

$$J_p = \alpha_y J_{py} + \alpha_z J_{pz}, \quad (23)$$

where

$$J_{py} = \frac{1}{\pi}\sum_{k=1}^{len(\omega)} \mathrm{tr}\left\{H_y(j\omega)H_y^{\mathrm{H}}(j\omega_k)\right\}\Delta\omega, \quad (24)$$

$$J_{px} = \frac{1}{\pi}\sum_{k=1}^{len(\omega)} \mathrm{tr}\left\{H_x(j\omega)H_x^{\mathrm{H}}(j\omega_k)\right\}\Delta\omega, \quad (25)$$

and

$$H_y(j\omega_k) \triangleq G_{yu}(j\omega_k)S(j\omega_k), \quad H_z(j\omega_k) \triangleq G_{zu}(j\omega_k)S(j\omega_k) \quad (26)$$
$$S(j\omega_k) \triangleq \left(I - G_{yu}(j\omega_k)K(j\omega_k)\right)^{-1}, \quad (27)$$

$\Delta\omega$ is the frequency spacing between consecutive points, and H denotes the conjugate transpose. The relative weighting between α_z and α_y determines the emphasis placed on the output verses the entire state vector. This cost maximizes performance, but has no guaranteed stability margin.

The Nyquist-based stability cost is given by

$$J_s = \frac{1}{\pi}\sum_{k=1}^{len(\omega)} W(\omega_k)\frac{1}{d^2(j\omega_k)}\Delta\omega \quad (28)$$

where

$$d(j\omega_k) = \frac{|1 + G_{yu}(j\omega_k)K(j\omega_k)|}{T(\omega_k)}, \quad (29)$$

and $T(\omega_k)$ corresponds to a 95% confidence interval at the frequency of interest,

$$T(\omega_k) = 1.96\sigma(\omega_k). \quad (30)$$

This is a slightly modified version of the Nyquist-based cost function found in [5]. It takes into account the stability criterion as well as the ability to handle model uncertainty.

Nyquist analysis for SISO systems is a graphical stability test that is based on a plot of the loop gain $G(j\omega)K(j\omega)$ along a frequency contour. For closed loop stability, the number of encirclements of the $(-1, 0)$ critical point must be equal to the number of open loop unstable poles. Since the system under consideration is open loop stable, we require there to be zero counterclockwise encirclements of the critical point for closed loop stability. The distance metric (29) is simply the magnitude of the distance to the critical point divided by the confidence interval. Taking a weighted sum of the inverse of this distance metric squared means that the cost function will decrease as the curve moves farther from the critical point and/or has a smaller variance.

The total cost is a weighted sum of the stability and performance costs,

$$J = \alpha J_p + \beta J_s. \quad (31)$$

Equation (31) quantifies the stability verses robustness control problem. The relative weighting between α and β determines the emphasis placed on performance verses stability robustness. The beam's controller will be tuned with this cost function using the beam's FRF and postulated variance data.

C. Sensitivity

The sensitivity is determined by taking the gradient of the cost functions with respect to the controller parameters. The output performance sensitivity for an arbitrary controller variable, p_i, is given by

$$\frac{\partial J_{py}}{\partial p_i} = \frac{2}{\pi} \sum_{k=1}^{len(\omega)} \mathrm{tr}\left\{ \mathrm{Re}\left[\frac{\partial}{\partial p_i} H_y(j\omega) \right] H_y^{\mathrm{H}}(j\omega_k) \right\} \Delta\omega, \tag{32}$$

where

$$\frac{\partial H_y}{\partial p_i} = G_{yu} \frac{\partial S}{\partial p_i}, \tag{33}$$

$$\frac{\partial S}{\partial p_i} = S G_{yu} \frac{\partial K}{\partial p_i} S, \tag{34}$$

$$\frac{\partial K}{\partial p_i} = \frac{\partial C_c}{\partial p_i} \Phi_c B_c + C_c \Phi_c \frac{\partial A_c}{\partial p_i} \Phi_c B_c + C_c \Phi_c \frac{\partial B_c}{\partial p_i}, \tag{35}$$

$$\Phi_c = (sI - A_c)^{-1}. \tag{36}$$

$\frac{\partial J_{py}}{\partial p_i}$ is similarly defined. The sensitivity of the stability cost with respect to p_i is

$$\frac{\partial J_s}{\partial p_i} = \frac{2}{\pi} \sum_{k=1}^{len(\omega)} W \frac{1}{d^2} \frac{1}{|1 + G_{yu} K|} G_{yu} \frac{\partial K}{\partial p_i} \Delta\omega, \tag{37}$$

where $\frac{\partial K}{\partial p_i}$ is defined in (35). This is a modified version of the sensitivity given by [5].

The complete sensitivity is given by

$$\frac{\partial J}{\partial p_i} = \alpha \left(\alpha_z \frac{\partial J_{pz}}{\partial p_i} + \alpha_y \frac{\partial J_{py}}{\partial p_i} \right) + \beta \frac{\partial J_s}{\partial p_i} \tag{38}$$

Each controller parameter, p_i, is modified according to the above total sensitivity functions such that the total cost function is locally minimized.

VII. NUMERICAL SIMULATIONS

Numerical simulations were performed on a lumped mass model with 55 elements. The input and output were non-colocated; the input was at node 10 (corresponding to the experimental location), and the output displacement was chosen to be at node 26. The baseline controller was developed around a ROM with 12 states and the parameters from this controller provided the initial values for the controller tuning. Nyquist plots for both controllers are shown for the nominal and perturbed plants.

A. Baseline Controller

The optimization gains for the LQR controller were set to be $Q = 5I_{12\times12}$ and $R = 1e-12$. The Kalman filter process and measurement noise covariances were set to $P = 10$ and $M = 1$, respectively. The closed loop response for the nominal system results in excellent performance. The Nyquist stability plot (see Figure 14), however, reveals that the system becomes unstable when a multiplicative perturbation of 0.93 is applied to the stiffness term. This is the same perturbation as was used to characterize the uncertainty in Section V.

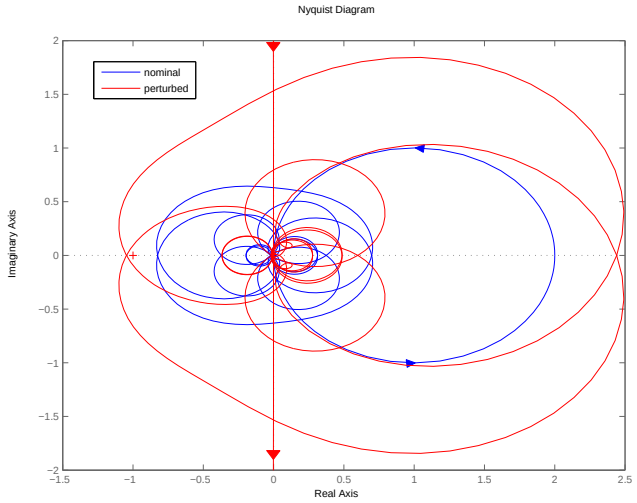

Fig. 14. Nyquist Plot for Baseline Controller with Perturbed and Unperturbed System

B. Robust Controller

The performance measure, z, was taken to be the state x, and therefore $C_z = I$ and $D_{zu} = 0$. The weighting $W(w_k)$ was taken to be unity when the real component of the loop gain was positive, and 20 when it was less than or equal to zero. Furthermore, the individual cost function weights were set to $\alpha_z = 1$, $\alpha_y = 1e10$, $\alpha = 1$, and $\beta = 1e4$.

From the Nyquist plot (Figure 15) we can see that the tuned controller regains closed loop stability in the presence of uncertainty.

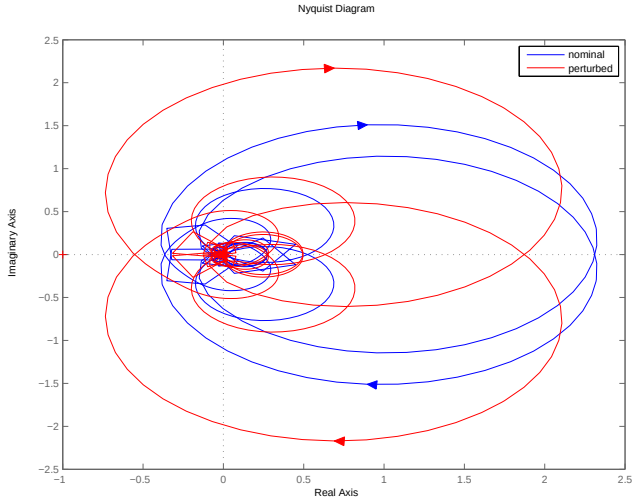

Fig. 15. Nyquist Plot for Tuned Controller with Perturbed and Unperturbed System

C. Comparison

The total, performance and robustness cost functions are shown in Table 1 for both the baseline and tuned controllers.

Table 1: Cost for Baseline and Tuned Controllers

	J-total	J_p-performance	J_s-stability
Baseline	3.3199e6	331.9889	8.9804e-8
Tuned	2.9413e6	294.1340	3.8619e-8

The tuned controller gave a reduction in both the performance and stability costs.

VIII. CONCLUSION AND FUTURE WORK

In conclusion, a baseline controller was tuned using a data-based cost function that includes a Nyquist-based stability robustness criterion with the more standard H_2 closed loop performance cost. This used FRF and variance data for the nominal plant to tune the controller. The tuned controller was applied to both perturbed and unperturbed lumped mass models of a free-free beam. The results showed that the closed loop system using the baseline controller became unstable in the presence of uncertain dynamics. However, the addition of the Nyquist-based cost for the controller optimization forced the closed loop system to remain stable for perturbations within the 95% confidence interval.

For future work, the authors plan to determine the response characteristics for various systems within the family of allowable plants (corresponding to the uncertainty). This will include various initial conditions as well as input and output disturbances. Furthermore, this work could be expanded and implemented for MIMO systems. It would also be interesting to apply the control theory to more complex flexible structures, such as the Deployable Optical Telescope.

IX. ACKNOWLEDGMENTS

The authors gratefully acknowledge the contribution of Jim Gooding and CSA engineering for collecting the Frequency Response Functions.

REFERENCES

[1] S. L. Lacy, V. Babuska, K. N. Schrader, and R. Fuentes, "System identification of space structures," in *American Control Conference*, Portland, OR, June 2005.

[2] K. Z. with J. C. Doyle, *Essentials of Robust Control*. Upper Saddle River, NJ: Prentice Hall, 1998.

[3] J. C. Doyle, "Guaranteed margins for LQG regulators," *IEEE Transactions on Automatic Control*, vol. 23, no. 4, pp. 756–757, August 1978.

[4] S. C. O. Grocott, J. P. How, and D. W. Miller, "Experimental comparison of robust H_2 control techniques for uncertain structural systems," *Journal of Guidance*, vol. 20, no. 3, pp. 611–614, 1997.

[5] G. J. W. Mallory, "Development and experimental validation of direct controller tuning for spaceborne telescopes," *PHD Thesis, Massachusetts Institute of Technology*, 2000.

[6] P. K. Stevens, "A generalization of the nyquist stability criterion," *IEEE Transactions on Automatic Control*, vol. 26, no. 3, pp. 664–669, 1981.

[7] D. J. Ewins, *Modal Testing: Theory and Practice*. Research Studies Press, 1984.

[8] S. S. Rao, *Mechanical Vibrations*, 3rd ed. Addison-Wesley Publishing Company, 1995.

[9] D. J. Inman, *Engineering Vibration*. Englewood CLiffs, New Jersey: Prentice Hall, 1994.

[10] P. M. Jenkins, *Mechanics of Materials Laboratory, ME* 354, University of Washington, January 2001.

[11] J. L. Junkins and Y. Kim, *Introduction to Dynamics and Control of Flexible Structures*, ser. AIAA Education Series. Washington, DC: American Institute of Aeronautics and Astronautics, Inc., 1993.